Articles

Synthesis and Self-Limited Electrochemical Doping of Polyacetylene Ionomers

Lei Gao, Dean Johnston,† and Mark C. Lonergan*

Department of Chemistry, The Materials Science Institute and the Oregon Nanoscience and Microtechnologies Institute, University of Oregon, Eugene, Oregon 97403

Received February 22, 2008; Revised Manuscript Received March 17, 2008

ABSTRACT: The synthesis, electrochemical characterization, and self-limited electrochemical doping of a family of soluble polyacetylene ionomers are reported. The conjugated ionomers (also known as conjugated polyelectrolytes) are synthesized by the ring-opening metathesis copolymerization of ionically functionalized cyclooctatetraenes with the nonionic trimethylsilylcyclooctatetraene. Sulfonate and alkylammonium derivatized polyacetylenes are reported with functional group densities ranging from 1 per 5 double bonds to 1 per 65 double bonds and weight-average molecular weights of 10−20 kDa. Electrochemically, the copolymers can be reversibly n- and p-doped, although not sequentially on the same polymer film, and their voltammetric behavior appears as a superposition of their constituent homopolymers. The extent of electrochemical doping becomes self-limited by the ion density built into the polymer when it is carried out in an appropriately charged polyelectrolyte-based electrolyte. More specifically, the extent of electrochemical p-doping for the anionic polyacetylene derivatives scales linearly with the density of ionic functional groups when carried out in tetrabutylammonium polystyrenesulfonate/CH_3CN. Similar results are seen for the n-doping of the cationic polyacetylene derivatives in poly(*N,N*-dimethyl-3,5-dimethylene piperidinium) hexafluorophosphate/CH_3CN. The self-limiting nature of the oxidation in the polystyrenesulfonate-based electrolyte greatly extends the potential stability window (to as much as 1.4 V vs SCE) of the polyacetylene anionomers without the same irreversible degradation observed in more conventional small ion electrolytes.

1. Introduction

Ionic functionality and mixed ionic/electronic transport has been an increasingly prominent theme in polymeric semiconductors for applications in areas such as light emission,[1–3] solar energy conversion,[4,5] and sensing.[6,7] Examples of these materials include blends of conventional conjugated polymers with polymer electrolytes[1,4,8] and single-component ionically functionalized materials known as conjugated ionomers or conjugated polyelectrolytes.[9,10] The single-component systems are distinguished by the absence of macrophase separation[11] and the need to control ion density through materials synthesis rather than blend formulation. In the undoped state, conjugated ionomers can have intrinsic ionic conductivity and the ability to transport injected electronic charge. Properties like these have led to applications such as polymer light-emitting electrochemical cells.[3] In the doped state, they can form internally compensated states where the injected charge is balanced by counterions covalently bound to the polymer backbone.[12,13] Central to understanding and exploiting the electrical properties of conjugated ionomers is the availability of materials with varied densities and signs of ionic functionality. A wide variety of different types of conjugated ionomers have been synthesized;[7] however, there has been limited work on developing families of conjugated ionomers with systematically varying ionic functional group density and charge.

The work presented herein has two primary goals. The first is to demonstrate the synthesis of a family of polyacetylene ionomers with a controlled density and type of ionic functionality. This ionomer synthesis is achieved through the ring-opening metathesis copolymerization of cyclooctatetraene (COT) monomers with appropriate functionality as shown in Scheme 1. The second goal is to use the copolymers to explicitly demonstrate self-limited electrochemical doping (SLED) as an important concept in the doping chemistry of conjugated ionomers. The demonstration of SLED is achieved using polyelectrolyte-based liquid electrolytes to control the supply of charge-balancing counterions and thereby mediate electrochemical doping.

Polyacetylene ionomers are being developed in our laboratory mainly to study novel electroactive junctions. These materials belong to the larger class of substituted polyacetylenes available

Scheme 1. Ring-Opening Metathesis Copolymerization To Yield Polyacetylene Ionomers, Which Are Shown as Idealized Structures

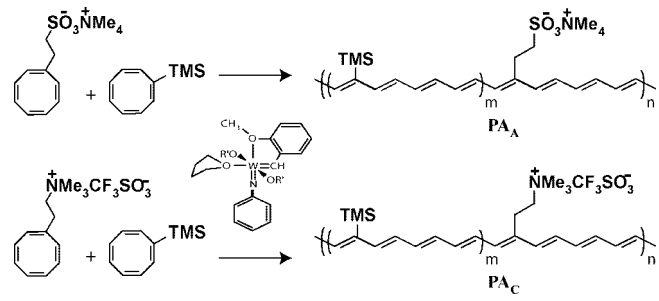

* To whom correspondence should be addressed.
† Present address: Department of Chemistry and Biochemistry, Otterbein College, Westerville, OH 43081.

10.1021/ma8004108 CCC: $40.75
Published on Web 05/17/2008

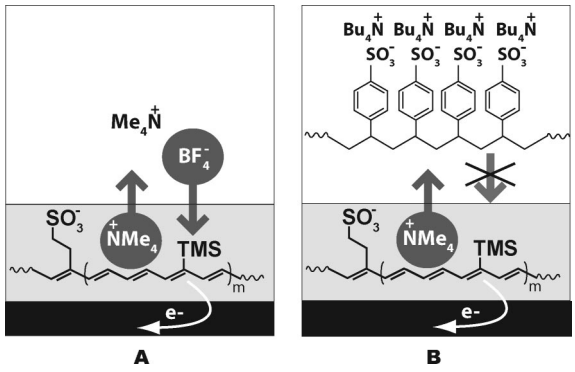

Figure 1. Schematic comparing the conventional electrochemical p-doping of an anionic polyacetylene ionomer with the self-limited electrochemical doping of the same polymer. (A) In a conventional electrolyte, oxidative p-doping can occur with the incorporation of an anion from the electrolyte or a loss of a cation from the conjugated ionomer. (B) In a polyanion-based electrolyte, oxidation can only occur with a loss of a cation from the polymer film, resulting in the oxidation level being limited by the available cations built into the polymer.

from the ring-opening metathesis polymerization (ROMP) of substituted cyclooctatetraenes (RCOTs).[14–16] We have used polyacetylene ionomers to demonstrate unidirectional current at junctions between mixed ionic/electronic conductors where there is a transition in the charge of the ion at the junction.[17] We have also used the concept of internal compensation to stabilize junctions between dissimilarly doped conjugated ionomers, enabling the fabrication of a doped pn junction diode.[18] Current rectification in these systems is poorly understood, and materials of varying ionic functional group density are needed to better probe the underlying mechanisms.

The control of doping chemistry is essential in the fabrication and study of interfaces and more complex structures based on doped conjugated polymers. Polyelectrolyte-mediated electrochemistry (PME) is a tool for controlling the doping of conjugated ionomers using polyelectrolyte-based electrolytes.[19,20] The principles of PME as applied to conjugated ionomers are derived from work using polyelectrolytes to access specific redox states in inorganic systems.[21] The SLED of conjugated ionomers is one application of PME. A key hypothesis regarding SLED is that the extent of doping will be controlled by the density of ionic functional groups built into the polymer structure. The concept is illustrated in Figure 1 by considering the electrochemical oxidative p-doping of a polyacetylene anionomer. Such p-doping requires either the incorporation of an anion from the electrolyte or the loss of cation from the polymer film. If a large polyanion, such as polystyrenesulfonate, is used for the electrolyte solution, p-doping is expected to be limited to the level that can be supported by the loss of cations from the film; the built-in ion content will control the ultimate doping level regardless of the electrode potential.

We have previously used PME to demonstrate the self-limited electrochemical p-doping of a polyacetylene anionomer to prevent deleterious overoxidation and the selective doping of one polyacetylene ionomer over another.[20] There has yet to be, however, an explicit demonstration that the level of doping is indeed controlled by the ion content built into the conjugated ionomer. The SLED concept has also not been demonstrated for the reductive n-type doping of conjugated cationomers. The materials synthesized herein make possible such demonstrations.

2. Results

2.1. Synthesis and Characterization. The tungsten alkylidene catalyst of Scheme 1 was used to initiate the ring-opening metathesis copolymerization of the monomer trimethylsilylcyclooctatetraene (M_{TMS}) with ionically functionalized COT monomers (M_X) to yield polyacetylene ionomers with varying ionic functional group density and charge. Two series of polymerizations were conducted. In the first, M_{TMS} was copolymerized with the anionically functionalized monomer tetramethylammonium 2-cyclooctatetraenylethylsulfonate (M_A). In the second, M_{TMS} was copolymerized with the cationically functionalized monomer (2-cyclooctatetraenylethyl)trimethylammonium triflate (M_C). Scheme 1 shows idealized segments of the resulting anionic and cationic polyacetylene copolymers: $PA_A^{F_x}$ and $PA_C^{F_x}$, respectively. Here, F_x is the mole fraction of ionic functional groups relative to the total number of ionic and TMS functional groups in the isolated polymers.

Before preparing bulk samples of the polymers, a series of test polymerizations were followed by ^{1}H NMR in $CDCl_3$. The primary goal of these experiments was to determine a reaction time for each of the two series of copolymerizations that would result in less than a 20% compositional drift in the monomer composition. Analysis of the time-dependent ^{1}H NMR spectra indicated that reaction times of 60 min for the PA_C series and 210 min for the PA_A series would keep compositional drift of the feedstock below the desired 20%. As with the homopolymerizations of M_A, M_C, and M_{TMS}, the ^{1}H NMR spectra also revealed very slow initiation of the tungsten alkylidene catalyst. The characteristic alkylidene resonance of the pure catalyst at 10.5 ppm[22] remained unchanged throughout the polymerization. Any propagating alkylidene was too dilute to be observed by ^{1}H NMR. Trimethyl(phenyl)silane was observed in the ^{1}H NMR as the only significant backbiting product. At the planned termination times, the molar amount of cycloextruded trimethyl(phenyl)silane was less than 15% of the molar amount of M_{TMS} consumed.

Bulk copolymerizations were carried out in $CHCl_3$. A series of anionic and cationic copolymers were made by varying the initial mole fraction of ionic monomer ($f_x = [M_X]_0/([M_X]_0 + [M_{TMS}]_0)$), as shown in Table 1. In all cases, precipitation of a strongly colored polymer was evident during the reaction. On the basis of the ^{1}H NMR data and the desire to minimize compositional drift, the copolymerizations were terminated by the addition of benzaldehyde at 210 min for polymerizations with M_A and at 60 min for polymerizations with M_C. The isolated polymers were purified by first removing excess M_{TMS} in vacuo followed by extensive washing with CH_3CN to remove catalyst residue and residual ionic monomer. The percent conversion based on gravimetric analysis of the isolated polymers was between 9 and 18% for PA_A and between 16 and 38% for PA_C (see Table 1). All of the isolated polymers were found to be sufficiently soluble in dimethylformamide (DMF) for solution phase characterization and thin film preparation by solution casting. The isolated polymers were characterized by ^{1}H NMR, UV/vis spectroscopy, gel permeation chromatography with refractive index and multiangle laser light scattering (MALLS) detection, and cyclic voltammetry as described below and in the Experimental Section.

The isolated polymers were dissolved in DMF-d_7 and characterized by ^{1}H NMR spectroscopy. All of the isolated polymers exhibited two broad and overlapping resonances in the region characteristic of the backbone protons in poly(RCOT)s: one near 7.2 ppm and the other near 6.6 ppm. The relative intensity of the upfield to downfield resonance was 2.5 $\pm$ 0.7 with no clear dependence on polymer composition. The polymers exhibited relatively sharp TMS resonances at 0.25 ppm and methylammonium resonances at 3.49 ppm for the PA_C series ($-N(CH_3)_3$) and 3.39 ppm for the PA_A series ($N(CH_3)_4$). The methylene proton resonances from the ionic side chains were broad and partially obscured by solvent DMF resonances in the range 2.5$-$3.0 ppm for PA_A. For PA_C, the methylene proton resonances were broad and at 2.7 and 3.5 ppm. The former was

Table 1. Summary of Data on Copolymerizations[a]

	$[C]_0$/mM	$[M_X]_0$/mM	$[M_{TMS}]_0$/mM	$[M_{tot}]_0$/mM	yield/%	f_x	F_x	M_w[b]/Da	λ_{max}[c]/nm
$PA_C^{0.19}$	2.5×10^1	4.0×10^1	2.0×10^2	2.4×10^2	17	0.17	0.19	1.8×10^4	520
$PA_C^{0.24}$	2.5×10^1	4.8×10^1	1.9×10^2	2.4×10^2	38	0.20	0.24	1.0×10^4	530
$PA_C^{0.61}$	2.5×10^1	8.1×10^1	1.6×10^2	2.4×10^2	16	0.34	0.61	1.5×10^4	560
$PA_C^{0.81}$	2.5×10^1	1.2×10^2	1.2×10^2	2.4×10^2	20	0.50	0.81	1.3×10^4	590
$PA_A^{0.06}$	4.0×10^1	1.5×10^2	5.0×10^2	6.5×10^2	18	0.23	0.06	1.8×10^4	530
$PA_A^{0.11}$	4.0×10^1	1.5×10^2	4.0×10^2	5.5×10^2	13	0.27	0.11	2.4×10^4	560
$PA_A^{0.20}$	4.0×10^1	1.5×10^2	3.0×10^2	4.5×10^2	12	0.33	0.20	9.5×10^3	570
$PA_A^{0.32}$	4.0×10^1	1.5×10^2	1.5×10^2	3.0×10^2	9	0.50	0.32	2.2×10^4	580

[a] $[C]_0$, $[M_X]_0$, $[M_{TMS}]_0$, and $[M_{tot}]_0$ are the initial concentrations of catalyst, ionic COT, TMS-COT, and total COT, respectively. The mole fraction of ionic monomer in the initial feedstock and of ionic functional groups in the isolated copolymer are f_x and F_x, respectively. [b] Weight-average molecular weight determined by MALLS. [c] In DMF solution.

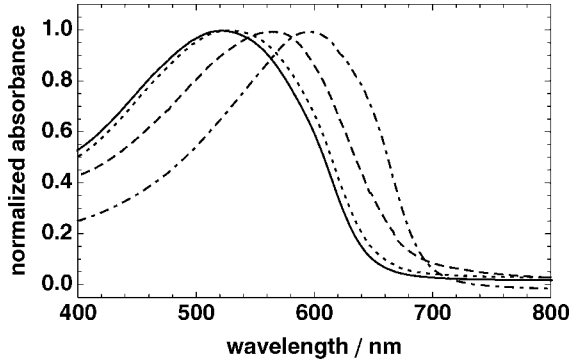

Figure 2. UV/vis absorption spectrum for the PA_C series of copolymers (solid: $PA_C^{0.19}$; dotted: $PA_C^{0.24}$; dashed: $PA_C^{0.61}$; dot-dashed: $PA_C^{0.81}$). The spectra are normalized by their absorption maxima.

obscured by solvent DMF resonances and the latter overlapped with the methylammonium resonances.

Integration of the ^{1}H NMR resonances for the ionic side chain and TMS group was used to determine the polymer composition. For the PA_C series, the combined integral of the methyl proton and methylene proton resonances near 3.5 ppm (I_{Me_3N,CH_2}) and the trimethylsilyl proton resonance at 0.25 ppm (I_{Me_3Si}) were used to determine $F_x = I_{Me_3N,CH_2}/[I_{Me_3N,CH_2} + (11/9)I_{Me_3Si}]$. For the PA_A series, the integrals of the methyl proton resonances for the tetramethylammonium and trimethylsilyl groups, I_{Me_4N} and I_{Me_3Si}, respectively, were used to determine $F_x = I_{Me_4N}/[I_{Me_4N} + (4/3)I_{Me_3Si}]$. The resulting compositions are tabulated in Table 1. The range of compositions correspond to approximately one ionic functional group per 5 double bonds ($PA_C^{0.81}$) to one per 65 double bonds ($PA_A^{0.06}$). Over the range studied, the polymer composition for the PA_C series was found to be enriched in ionic monomer relative to the initial monomer feedstock ($F_x > f_x$), with the greatest percent discrepancies at high f_x. The reverse was observed for the PA_A series with the polymer found to be depleted of ionic monomer relative to the initial monomer feedstock ($F_x < f_x$), with the greatest percent discrepancies at low f_x. The actual compositional drift of the monomer feedstock during each polymerization was estimated from the yield and composition of the isolated polymers. In each case, the monomer composition was estimated to vary less than 20% over the course of the intentionally terminated polymerizations, as expected from the test polymerizations monitored by ^{1}H NMR.

The UV/vis spectra of solutions of the polymers in DMF were collected. All exhibited a single broad absorbance peak as shown in Figure 2 for the PA_C series. In airfree solutions, this absorbance peak was not observed to shift with time as has been observed in other initially isolated poly(RCOTs) due to a *cis* to *trans* isomerization.[16] The wavelength of maximum absorbance, λ_{max}, was in the range of 520−600 nm for all of the polymers, and it was observed to red shift with increasing ionic monomer content in both the anionic and cationic copolymer (see Table 1). The shape of the absorbance peaks was similar in all cases with a slight narrowing as the ionic monomer content increased over the range studied.

The polymers were also characterized with gel permeation chromatography using both refractive index and multiangle laser light scattering (MALLS) detection. The elution behavior of the copolymers was first compared to that of the homopolymers of M_A, M_C, and M_{TMS} synthesized under similar conditions. A Waters Styragel HR4 column with a nominal molecular weight range of 5×10^3−6×10^5 Da and DMF as an eluent were used for the comparison. The homopolymer of M_A eluted at the column volume of 4 mL (also true with Styragel columns of other molecular weight ranges) due to strong repulsions between this anionic polymer and residual negative charge on the stationary phase; the homopolymer of M_C did not elute even with the addition of a background electrolyte (tetrabutylammonium triflate or tetramethylammonium triflate) due to strong electrostatic adsorption to the stationary phase, and the homopolymer of M_{TMS} eluted near 8 mL (for comparison, polystyrene of MW = 10^4 Da eluted near 10 mL). The PA_A copolymers all eluted as a single peak near 5 mL and in between that of the homopolymers of M_{TMS} and M_A. No detectable polymer eluted from the PA_C copolymer samples.

MALLS was used to estimate the molecular weights of the copolymers. The measurements were performed at 788 nm, and optical absorption from the polymer at this wavelength was determined to have a negligible effect. The MALLS detector was used inline following the Styragel column for analysis of the PA_A copolymers and in batch mode for the PA_C copolymers as they could not be separated on the columns due to irreversible adsorption. Analysis of the scattering measurements yielded weight average molecular weights M_w in the range of 10−20 kDa with no systematic dependence on composition or polymerization conditions (see Table 1). The PA_A copolymers yielded apparent polydispersities from 1.3 to 1.9 systematically increasing with M_{TMS} content. The term apparent is used because separation may not have been on the basis of size exclusion alone due to additional contributions from electrostatic interactions. As the PA_C copolymers could not be separated by size exclusion chromatography, no polydispersities were calculated.

2.2. Conventional Electrochemistry. The oxidative (p-type) and reductive (n-type) doping of the polyacetylene copolymers were studied using cyclic voltammetry. Thin solid films between 1 and 5 μm on glassy carbon electrodes were electrochemically cycled in 0.075 M tetramethylammonium tetrafluoroborate ($TMABF_4$)/CH_3CN electrolyte. For each material, n- and p-doping cycles were conducted on separately prepared films. Each film was sequentially cycled through the doping and undoping process six times at two different scan rates, as shown in Figure 3 for anionic and cationic polymers of similar ionic functional group density: $PA_A^{0.20}$ and $PA_C^{0.19}$. The voltammograms were normalized by dividing the current by the scan rate, as appropriate for a redox species immobilized on an electrode.[23] Note that the abscissa for each plot spans 1 V in electrode

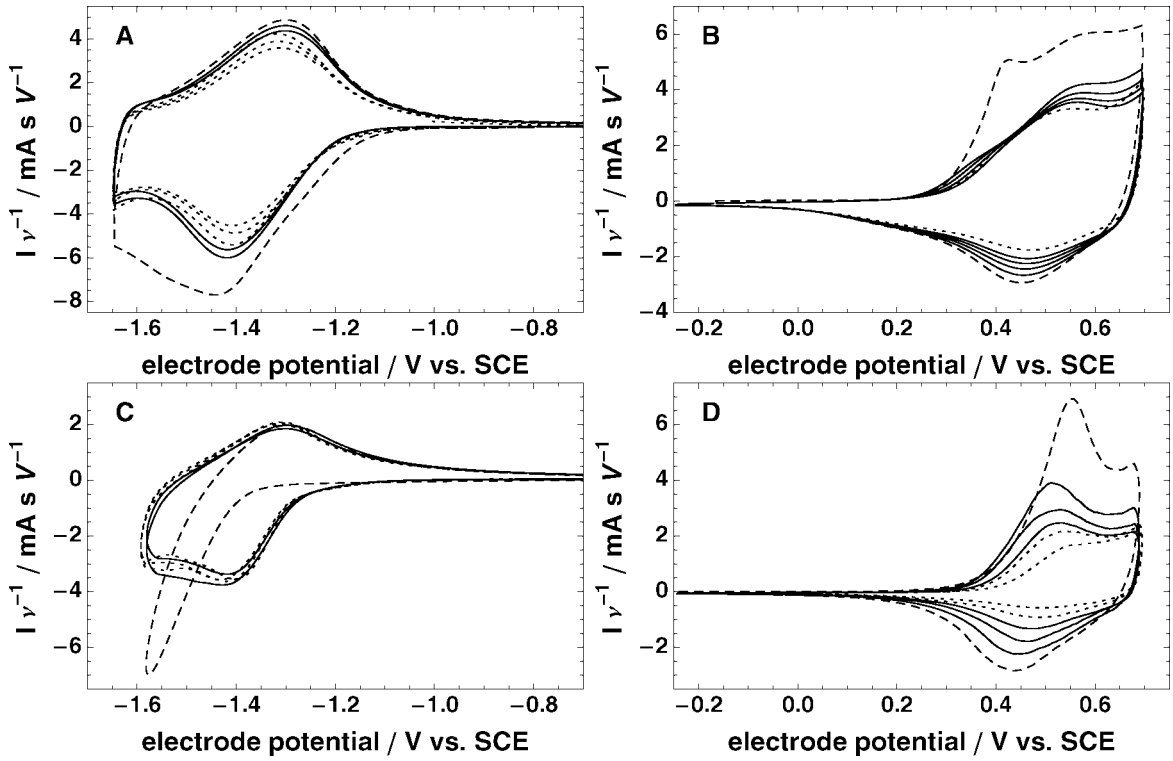

Figure 3. Cyclic voltammograms for the separate n- and p-doping of $PA_A^{0.20}$ (A and B, respectively) and $PA_C^{0.19}$ (C and D, respectively). The n-doping and p-doping voltammograms for each polymer were collected on separate films in 0.075 M Me_4NBF_4/CH_3CN. The dashed line in each is the first cycle at 20 mV s^{-1}. The solid and dotted lines are subsequent cycles: first at 20 mV s^{-1} and then at 10 mV s^{-1}, respectively. Within the sets of solid-line and dotted-line voltammograms, the scan order is apparent from the fact that the intensity decreased slightly with each cycle. The current (I) is normalized by the scan rate (ν).

potential so that the shapes of the various voltammograms can be readily compared.

The first cycle collected on each of the polymer films (dashed lines in Figure 3), whether it be to the n-doping or p-doping side, was distinctly different from subsequent scans. After this initial break-in cycle, the shape of the voltammogram was observed to change little although the amplitude of the voltammogram continuously decreased. The polymers could be reversibly n- and p-doped when these processes were conducted independently. Integration of the voltammograms indicated that the extent of doping decreased by less than 5% for each cycle with one exception: the extent of doping decreased 15% upon each p-doping cycle for the PA_C copolymers. The more rapid decay of the p-doping wave for the PA_C copolymers is evident for $PA_C^{0.19}$ in Figure 3D.

For all of the polymers studied, the cycling stability greatly decreased when the n- and p-doping processes were alternately cycled on a single film, as shown in Figure 4 for a film of $PA_A^{0.20}$. The n- and p-doping waves on the first cycle were observed to be similar to the voltammograms shown in Figure 3, but there was a notable difference on the second cycle. The p-doping wave showed a much larger anodic current early in the p-doping wave, and the n-doping wave was clearly chemically irreversible. By the third cycle, the sample had lost nearly all of its electroactivity. Similar results were observed for the other copolymers.

The n-doping and p-doping waves were observed to depend more strongly on polymer composition when it was possible to form an internally compensated state than when an additional counterion had to be incorporated upon doping. Figure 5 overlays the n- and p-doping voltammograms collected at 10 mV s^{-1} for all of the polymers studied. Figures 5A,D show the processes that required the net incorporation of an additional counterion upon doping (n-doping of PA_A and p-doping of PA_C),

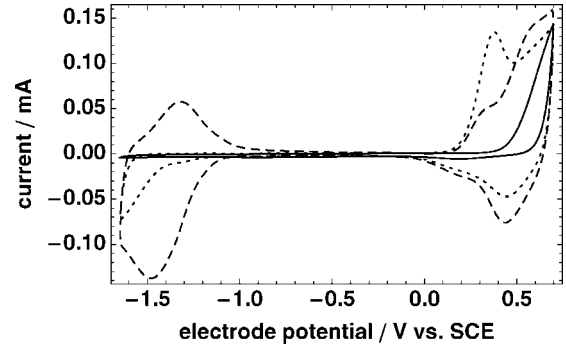

Figure 4. Cyclic voltammogram for a $PA_A^{0.20}$ film swept over both the n- and p-doping waves in 0.075 M Me_4NBF_4/CH_3CN. The scan rate is 20 mV s^{-1}. The scan was started by sweeping positive from 0 V vs SCE. The cycle order is dashed, dotted, solid.

and here, a strong dependence on polymer composition was not observed. The potentials of peak cathodic and anodic current, E^p_{cath} and E^p_{an}, respectively, for the n-doping of the PA_A series varied less than 50 mV from their average over all of the PA_A polymers (Figure 5A). For all but one of the polymers, the E^p_{cath} and E^p_{an} for the p-doping of the PA_C series varied less than 50 mV from their average over all of the PA_C polymers (Figure 5C). The one exception was for the p-doping of the most highly concentrated PA_C sample $PA_C^{0.81}$. In this case, the E^p_{cath} and E^p_{an} were shifted more significantly: 50 and 100 mV, respectively, from the mean values of the other PA_C copolymers.

The voltammograms for the p-doping of PA_A and n-doping of PA_C, where it is possible to form an internally compensated state, were much more strongly dependent on polymer composition (Figures 5B,C). The shape of the voltammogram changed with increasing ion content as two doping waves became evident. For the case of PA_A, a single wave in the vicinity of

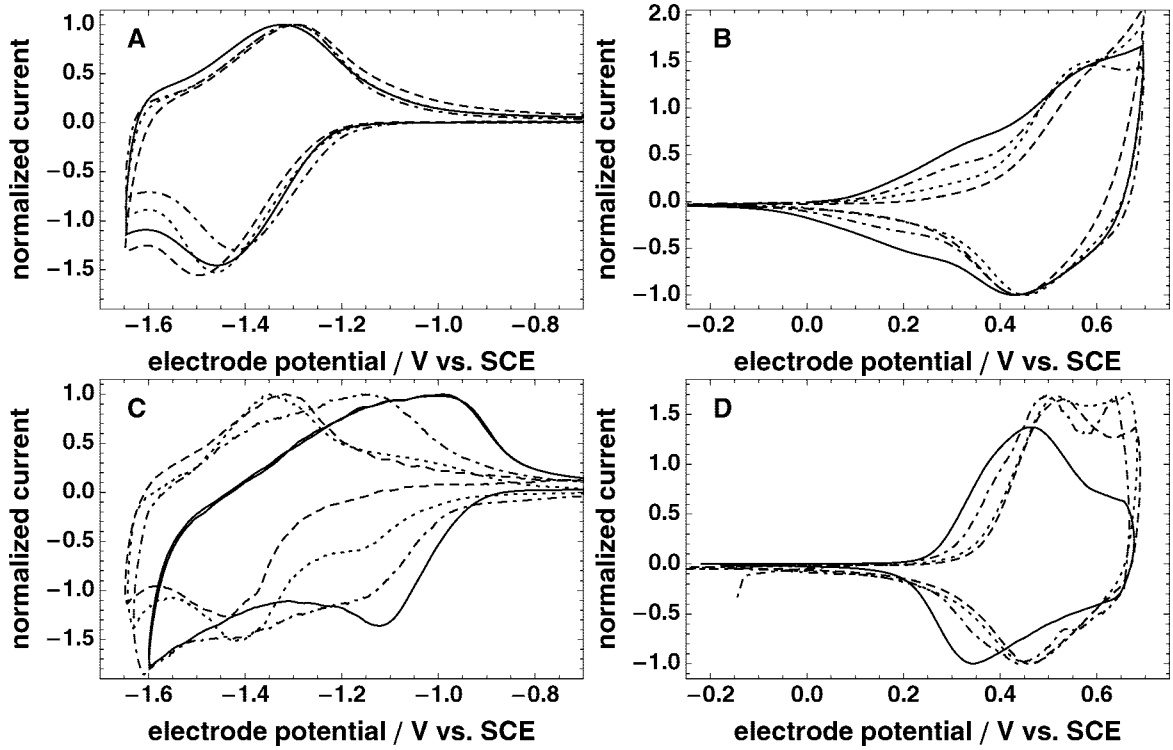

Figure 5. Comparison of the n-doping (A) and p-doping (B) cyclic voltammograms for the PA_A series copolymers (solid: $PA_A^{0.32}$; dot-dashed: $PA_A^{0.20}$; dotted: $PA_A^{0.11}$; dashed: $PA_A^{0.06}$) and the n-doping (C) and p-doping (D) voltammograms for the PA_C series copolymers (solid: $PA_C^{0.81}$; dot-dashed: $PA_C^{0.61}$; dotted: $PA_C^{0.24}$; dashed: $PA_C^{0.19}$). For each copolymer, the n-doping and p-doping voltammograms were collected on separately prepared films, and all of the voltammograms were collected in 0.075 M Me_4NBF_4/CH_3CN at 20 mV s^{-1}. The voltammograms are normalized by the peak anodic current for the n-doping voltammograms (A and C) and by the peak cathodic current for the p-doping voltammograms (B and D).

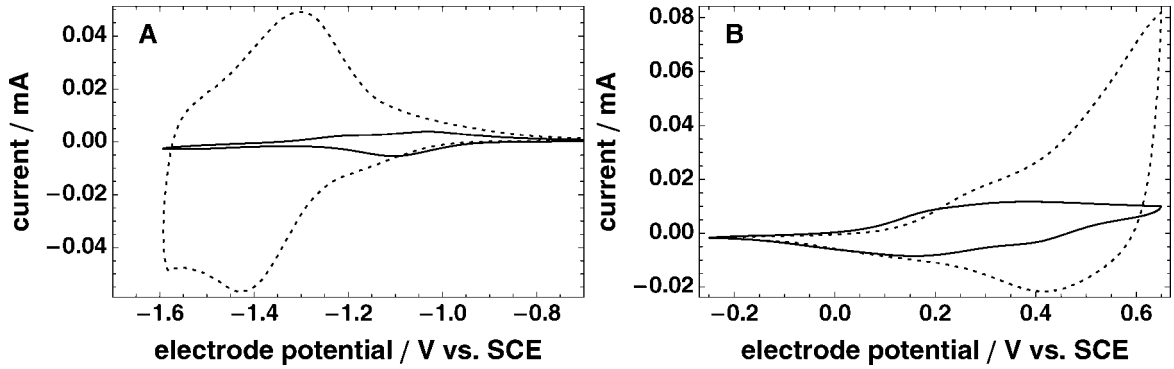

Figure 6. Demonstration of polyelectrolyte mediated electrochemistry. Part A compares the cyclic voltammograms of a solid film of $PA_C^{0.24}$ first swept in 0.1 M PDDP/CH_3CN (solid line) and then in 0.075 M NMe_4BF_4/CH_3CN (dashed line). Part B compares the cyclic voltammograms of a solid film of $PA_A^{0.20}$ first in 0.1 M PSS/CH_3CN (solid line) and then in 0.1 M NBu_4BF_4/CH_3CN. The scan rate is 20 mV s^{-1}.

0.5 V vs SCE dominated the voltammogram at low ion concentration, and a new wave near 0.3 V vs SCE grew in as the ion concentration was increased. For the case of PA_C, the low ion concentration voltammogram was dominated by a wave in the vicinity of −1.4 V vs SCE with a new wave growing in near −1.1 V vs SCE as the ion concentration increased. As discussed further below, the lower energy of the two waves in each case (0.3 V vs SCE for p-doping PA_A and −1.1 V vs SCE for n-doping PA_C) is assigned to a doping process involving an internally compensated state formed in polymer regions rich with ionically functionalized monomer. The higher energy wave is assigned to a noninternally compensated state in regions rich with M_{TMS}.

2.3. Self-Limited Electrochemical Doping. The cyclic voltammograms for thin solid films of the copolymers were collected in polyelectrolyte-based liquid electrolytes to explore the concept of self-limited electrochemistry. Acetonitrile solutions of the anionic polyelectrolyte tetrabutylammonium polystyrenesulfonate (PSS) and cationic polyelectrolyte poly(*N,N*-dimethyl-3,5-dimethylene piperidinium hexafluorophosphate) (PDDP) were used to study the p-doping of PA_A and n-doping of PA_C, respectively. Figure 6A compares the n-doping of $PA_C^{0.24}$ in 0.1 M PDDP/CH_3CN with that in 0.075 M $TMABF_4/CH_3CN$, and Figure 6B compares the p-doping of $PA_A^{0.20}$ in 0.1 M PSS/CH_3CN with that in 0.1 M tetrabutylammonium tetrafluoroborate (Bu_4NBF_4)/CH_3CN. The data shown in each part of Figure 6 were collected on a single polymer film that was first scanned in the macromolecular electrolyte and then in small-ion electrolyte. For both doping processes, it can be seen that the voltammetric wave is much smaller in the macromolecular electrolyte relative to the small ion electrolyte. For the n-doping of $PA_C^{0.24}$ in PDDP, a single doping wave at −1.1 V vs SCE was seen. For the p-doping of $PA_A^{0.20}$ in PSS, a single doping wave at 0.25 V vs SCE was seen. For each polymer, the use of

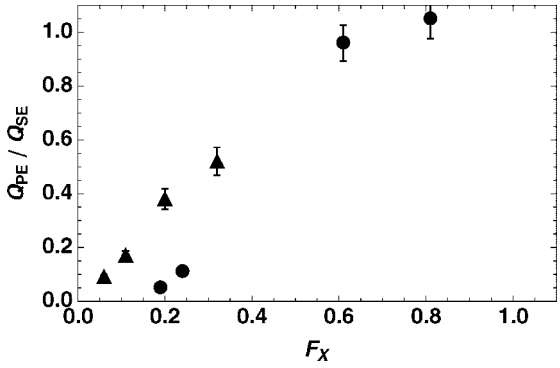

Figure 7. Illustration of self-limited doping. The solid triangles are the ratio of charge for the p-doping of the PA_A series of copolymers in 0.1 M PSS/CH_3CN vs 0.1 M Bu_4NBF_4/CH_3CN. The solid circles are the ratio of charge for the p-doping of the PA_C series of copolymers in 0.1 M PDDP/CH_3CN vs 0.075 M Me_4NBF_4/CH_3CN.

the macromolecular electrolyte results in the selective doping of the lowest energy of the two doping processes observed in small ion electrolyte.

The relative extent of doping in the macromolecular vs small molecule electrolyte for the entire PA_A and PA_C series was calculated by integrating the voltammograms to determine the total charge injected into the polymer. The anodic and cathodic waves for each voltammogram were integrated and their average used to determine the charge Q. Figure 7 compares the ratio of the charge injected into the polymer in the polyelectrolyte-based liquid electrolyte (Q_{PE}) to that in the small molecule electrolyte (Q_{SE}) for the p-doping of PA_A and n-doping of PA_C. For PA_A, the ratio Q_{PE}/Q_{SE} was observed to increase linearly with increasing F_x over the range studied. For PA_C, the same increase with F_x was observed, but the $Q_{PE}/Q_{SE}-F_x$ relation did not extrapolate to zero. Furthermore, Q_{PE} and Q_{SE} were observed to be statistically indistinguishable from unity at the highest two concentrations for the PA_C series.

The p-doping of the PA_A series copolymers in Bu_4NBF_4 vs PSS was also explored at more extreme positive potentials in an effort to further explore the self-limiting principle. The potential stability window of the PDDP/CH_3CN electrolyte precluded a similar comparison for the n-doping of the PA_C copolymers. A single polymer film was first cycled multiple times in 0.1 M PSS/CH_3CN and then in Bu_4NBF_4/CH_3CN. In PSS, the film was scanned in blocks of three cycles with each block at a different scan rate to assess any kinetic limitations. Figure 8A shows scans at 20, 10, and 5 mV s^{-1} normalized by the scan rate ν as is standard for immobilized electroactive films. The cycles shown correspond to the 10th, 13th, and 16th overall cycles. The normalized voltammograms nearly superimposed indicating that the film could be reversibly cycled through the very large potential excursion used. Even after 16 cycles, the film had not lost any substantial degree of electroactivity. The peak-to-peak separation was observed to increase some with scan rate indicating kinetic limitations, in particular at 20 mV s^{-1}. The agreement between the normalized scan-rate-dependent voltommograms was the poorest at the most positive potentials, and the current never dropped to levels associated with pure capacitive charging. There was also an increasing lag in the reversal of the current in response to the potential reversal at 1.35 V vs SCE as the scan rate increased. Following a total of 20 cycles in PSS/CH_3CN, the polymer film was then transferred to Bu_4NBF_4/CH_3CN and cycled over the same potential range (Figure 8b). The first cycle in this electrolyte exhibited a very large anodic current leading to the irreversible overoxidation of the polymer. By the third cycle, the polymer had essentially lost all of its electroactivity.

3. Discussion

3.1. Synthesis and Characterization. The results support the formation of polyacetylene derivatives with a controlled density of anionic or cationic functional groups. In particular, the spectroscopic data support the formation of polyacetylene ionomers in the predominately *trans* configuration. The structure of the monomers necessitates the initial formation of a *cis* configuration. Presumably, the *cis* form was not observed because it isomerized in solution before characterization. The backbone ^1H NMR resonances for the synthesized copolymers were observed exclusively in the 6−7 ppm region, consistent with previous results on predominately *trans*- poly(RCOT)s.[16] For comparison, *cis*-poly(RCOT)s are reported to exhibit resonances upfield of 6 ppm.[16] The visible absorption data are also consistent with the *trans* configuration. The range of λ_{max} values (520−600 nm) for the solution phase copolymers fell in the range of other predominately *trans*-poly(RCOTs). For comparison, the homopolymer of M_{TMS} in THF is reported to have a $\lambda_{max} = 540$ nm in the *trans* form and a $\lambda_{max} = 380$ nm in the *cis* form.[16] The homopolymers of M_A and M_C have only been isolated in the *trans* form with values of λ_{max} near 620 nm.[24] The TMS group presents more steric hindrance near the polymer backbone than either of the ionic side chains, thereby resulting in a greater disruption of the π conjugation and a blue shift in λ_{max}. Consistent with this, the λ_{max} for the copolymers was observed to systematically blue shift with increasing TMS content.

The MALLS data verify the macromolecular structure of the polymers. The M_w range of 10−20 kDa determined by light scattering analysis is low relative to nonionic poly(RCOT)s synthesized using the tungsten alkylidene catalyst employed herein,[16] but it is still higher than might be expected on the basis of the monomer to catalyst ratios employed. In many cases, ROMP initiated by transition metal alkylidene catalyts is known to yield living or controlled polymerizations.[25,26] In the case of an ideal controlled polymerization, the molecular weight at 100% conversion would be determined by the monomer to catalyst ratio. The polymerizations herein were conducted at very low monomer to catalyst ratios ranging from 5:1 to 14:1, which would yield maximum molecular weights in the range of 1−4 kDa for a controlled polymerization. The ^1H NMR data and previous work[27] on the polymerization of RCOTs using the same tungsten catalyst show that only a small fraction of the catalyst initiates and hence participates in the polymerization. Under these circumstances, higher molecular weights are attainable because of the reduction in the number of propagating species. In fact, a small monomer to catalyst ratio was used precisely to accelerate the overall polymerization given the very slow initiation. As there is never a complete depletion of the monomers for the polymerizations herein, the molecular weight distribution is expected to be governed by termination processes including intentional quenching of the polymerization, true termination reactions, and precipitation. The latter process was argued as an important pseudotermination step in controlling the molecular weight of poly(M_A),[27] and precipitation was clearly evident in all of the copolymerizations studied herein. The molecular weights observed correspond to between 170 and 510 double bonds per chain.

The copolymerization method provides the desired control over ion concentration. Not surprisingly, the polymer composition is not directly given by that of the monomer feedstock. The general trend is as expected in the zero-order approximation of an ideal coplymerization. In this case, the relative homopropagation rates of the monomers[27]—M_C > M_{TMS} > M_A—predict $F_x > f_x$ for the PA_C series and $F_x < f_x$ for the PA_A series, as is observed. The presence of backbiting reactions and the limited set of compositions studied preclude a detailed

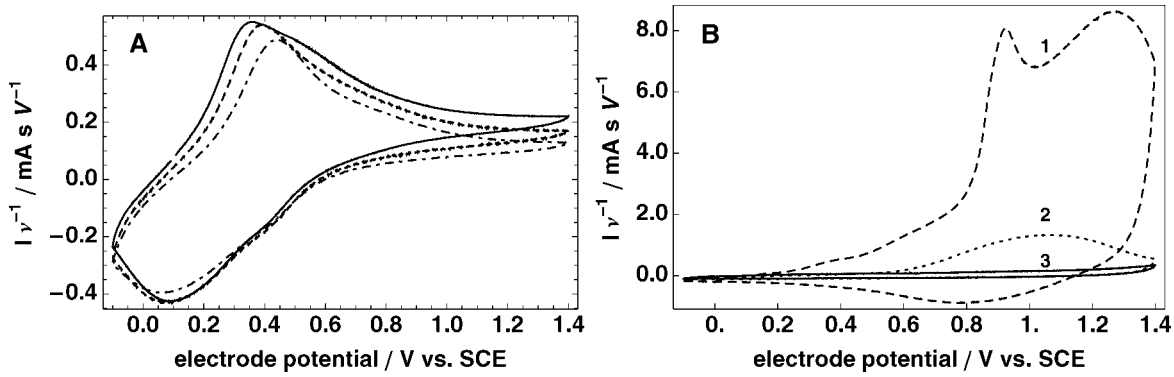

Figure 8. Voltammograms of $PA_A^{0.20}$ scanned first in 0.1 M PSS/CH_3CN (A) and then in 0.1 M $TBABF_4$/CH_3CN (B). The PSS voltammograms in (A) were collected at 5 mV s^{-1} (solid line), 10 mV s^{-1} (dashed line), and 20 mV s^{-1} (dot-dashed line). The scans are the 10th, 13th, and 16th cycles in a 20-cycle experiment with blocks of varying scan rate in PSS. The voltammograms in (B) were collected at 20 mV s^{-1} immediately following cycling in PSS and on the same film as in (A). The cycle order is dashed, dotted, solid. In both (A) and (B), the current is normalized by the scan rate ν.

analysis of the F_x–f_x composition curve to calculate reactivity ratios.

There is little advantage to the putative copolymerizations if for some reason they yield a mixture of homopolymers. Hence, it is worth explicitly discussing the copolymeric nature of the products. Although unlikely, homopolymers could theoretically result from very large reactivity ratios. In addition, there is a point at which the minor monomer component becomes so dilute that it is statistically improbable or impossible for each polymer chain to contain both monomers. The GPC data argue against homopolymer formation. For the PA_C series, homopolymer formation is ruled out by the fact that no material was observed to elute from the size exclusion column, whereas separately prepared poly(M_{TMS}) was observed to elute under identical chromatographic conditions. For the PA_A series, homopolymer formation is ruled out by the fact that the copolymers were observed to elute as a single peak at greater than the column volume, whereas separately prepared poly(M_A) was observed to elute at the column volume due to strong electrostatic interactions. The UV/vis data also argue against homopolymer formation. In particular at compositions near $F_x = 0.5$, the solution UV/vis absorption spectrum for a homopolymer mixture would be expected to appear clearly as a superposition of two homopolymer spectra. Instead, a single peak was observed in all cases with λ_{max} steadily shifting with F_x. In regard to monomer dilution relative to chain length, the minimum average number of ionic functional groups per polymer chain for any of the polymers is 4 ($PA_A^{0.06}$) based on the estimated number-average molecular weight and composition data. Given that there is expected to be a distribution in both chain length and ionic monomer content, the $F_x = 0.06$ is approaching the limit where some pure M_{TMS} chains become inevitable.

3.2. Conventional Electrochemistry. The cyclic voltammetry of thin films of conjugated polymers can be used to probe both the energetics and kinetics of the doping process. Herein, we are primarily interested in the energetics, and consequently we focus on voltammograms collected at scan rates sufficiently slow to minimize kinetic complications. In the absence of such complications, the shape of the voltammogram is not expected to depend on ν, aside from a normalization factor of ν^{-1}.[23] The solid and dotted lines closest together in each of the families of voltammograms shown in Figure 3 are sequential scans with the solid collected twice as fast as the dotted. For most all of the polymers studied, there was only a minor dependence on scan rate below 20 mV s^{-1}. Typically, the E_{an}^p and E_{cath}^p varied by less than 15 mV with a doubling of the scan rate. The notable exception was in the p-doping of the PA_C series where changes due to the time scale of the experiment were convoluted by poor cycling stability, as shown for the p-doping of $PA_C^{0.19}$ in Figure 3D.

The slow-scan voltammetry of the copolymers derives closely from that of the constituent homopolymers.[20] This can be most clearly seen by considering the p-doping of the PA_A series and the n-doping of the PA_C series. Figure 9 compares the voltammogram for the p-doping of $PA_A^{0.20}$ and for the n-doping of $PA_C^{0.24}$ with that of the homopolymers of M_{TMS} and either M_A or M_C as appropriate. Also shown is a linear combination of the homopolymer voltammograms. The relative scaling of the homopolymer voltammograms was derived from a nonlinear least-squares fit of their linear combination to the copolymer voltammogram. The qualitative agreement of this linear combination to the experimental copolymer data demonstrate that the p-doping of PA_A and the n-doping of PA_C can both be seen as a superposition of processes. This suggests the existence of two electrochemically distinct regions of the copolymer films: one behaving as the homopolymer of M_{TMS} and the other as the homopolymer of either M_A or M_C as appropriate.

The separation between the doping processes seen in Figure 9 is due to the difference in the mechanics of maintaining charge neutrality. The n-doping of poly(M_C) and the p-doping of poly(M_A) in conventional electrolytes have been previously shown to yield an internally compensated state.[20] Charge neutrality is maintained by the loss of a counterion from the polymer film as opposed to the incorporation of an ion from the electrolyte as is required for the doping of the homopolymer of M_{TMS}. The relative energetics of losing a counterion as opposed to incorporating a counterion into the low-dielectric polymer film results in the internally compensated doping processes occurring at a lower energy. Charge is first and most easily injected into sites where there is a counterion available for internal compensation. Once these counterions are no longer available, doping proceeds as a higher energy process involving the incorporation of counterions. The p-doping of poly(M_C) and n-doping of poly(M_A) always require the incorporation of an ion so these processes appear as a single doping wave in the voltammogram with much less dependence on the density of ions built into the polymer structure (Figures 5A,D).

The cycling behavior of the copolymers is similar in many ways to our previous measurements on poly(M_A) and poly(M_C).[20] As is typical with conjugated polymers, all of the copolymers exhibited a break-in cycle as has been discussed elsewhere.[28–30] With the exception of the p-doping of the PA_C series, the observed cycling stability for the copolymers (less than 5% loss per cycle) is only slightly poorer

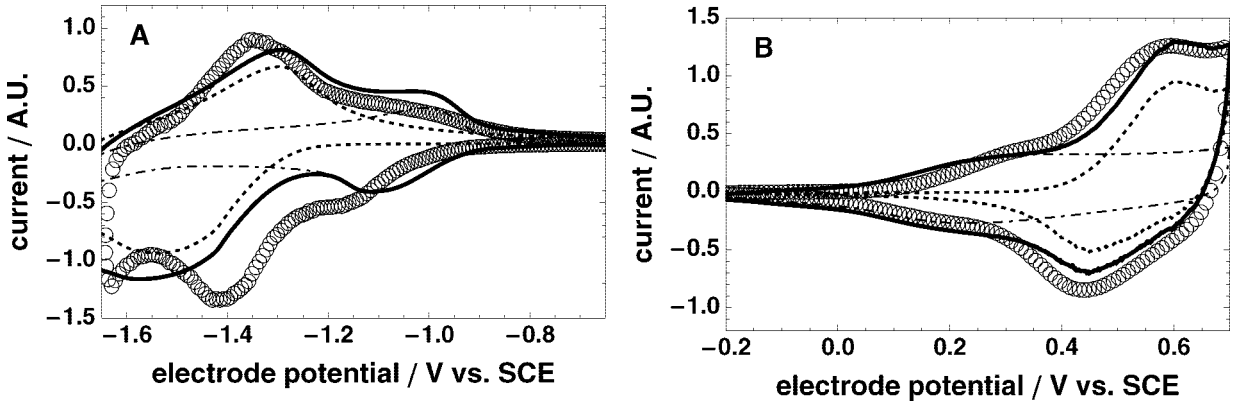

Figure 9. Comparison of the cyclic voltammogram of representative copolymers with that of their constituent homopolymers. Part A compares the n-doping voltammogram of $PA_C^{0.24}$ (circles) with that of the homopolymers of poly(M_{TMS}) (dotted line), poly(M_C) (dash-dot line), and a linear combination of the two. Part B compares the p-doping voltammogram of $PA_A^{0.20}$ (open circles) with that of the homopolymers of poly(M_{TMS}) (dotted line), poly(M_A) (dash-dot line), and a linear combination of the two (solid line).

that for the homopolymers of PA_A and PA_C (less than 2% loss per cycle).[20] This difference could simply be due to differences in experimental conditions because the cycling stability is very sensitive to oxygen or dissolved water. Some questions still remain regarding the full cycling behavior of the copolymers and parent homopolymers. Poly(M_C) is unusual in this group in that it can be reversibly cycled through both the n- and p-doping waves. Poly(M_A), on the other hand, shows some electroactivity at negative potentials, but not a clean reversible n-doping wave as seen for poly(M_C) and the copolymers. Cycling poly(M_A) to potentials negative of approximately -1 V vs SCE strongly influences the shape of p-doping wave in a manner very similar to that observed in the copolymer voltammogram of Figure 4. A relatively sharp peak grows into the voltammogram early in the second p-doping wave following the first large negative potential excursion. The details of the full cycling behavior are not fully understood, but the dependence of the behavior on the charge and density of the ions built into the polymer suggests that the mechanics of ion motion play a role. The ionic content of the polymer can potentially influence the availability of ions both directly and indirectly through changes in the permeability of the material. The availability of ions can in turn drastically affect the kinetics of various electrochemical processes including reversible doping and polymer overoxidation. A more detailed understanding of these processes awaits electrochemical quartz crystal microbalance and spectroelectrochemical measurements.

3.3. Self-Limited Electrochemical Doping. The ability of conjugated ionomers to undergo doping without requiring the incorporation of a counterion can be exploited in their self-limited doping.[20] The results of both Figures 6 and 7 demonstrate this principle. Consider first the p-doping of PA_A in PSS. In this case, doping can only occur with the loss of cations from the polymer film because the PSS anion is too large to be incorporated. Only the low-energy doping process is observed in the PSS voltammogram because the remainder of the doping wave observed in Bu_4NBF_4 requires the incorporation of an anion into the polymer film (see Figure 6A). The selective doping of the low-energy process in PSS and the fact that its magnitude scales with F_x further supports its assignment to the formation of an internally compensated state. In PSS-based electrolyte, the density of charge injected into the polymer upon voltammetric cycling is controlled by the density of exchangeable cations built into the polymer film. The extent of doping (Q_{PE}) relative to the full depth possible (Q_{SE}) is determined by the polymer composition: Q_{PE}/Q_{SE} scales linearly with F_x. This is in contrast with the conventional means of controlling the depth of electrochemical doping, which is through the control of electrode potential. The case of n-doping of PA_C in PDDP is similar. Here, doping requires the loss of an anion from the film because the PDDP cation is too large to be incorporated into the polymer film. Like PA_A in PSS, the Q_{PE}/Q_{SE} ratio for the n-doping of PA_C in PDDP increases with F_x, but unlike the PA_A case, the $Q_{PE}/Q_{SE}-F_x$ relation does not extrapolate through zero. This suggests that there is a portion of counteranions built into the film that are not accessible to the doping process. It is also seen that Q_{PE}/Q_{SE} for both $PA_C^{0.61}$ and $PA_C^{0.81}$ are to within error unity. In our previous experiments on the homopolyer of M_C, it was shown that the maximum reversible doping density is substantially less than the ion density.[20] The fact that poly(M_C) contains more ions than needed to support full doping means that the maximum doping level in the self-limited case can be achieved at less than $F_x = 1$, apparently by at least $F_x = 0.61$ in the PA_C series.

One significant advantage of SLED is the ability to prevent irreversible redox processes that degrade the polymer. Polyacetylene[31] and other conjugated polymers[32–34] are known to undergo an irreversible overoxidation if subjected to sufficiently positive potential excursions. This overoxidation is shown clearly in Figure 8B for $PA_A^{0.20}$ with polymer degradation complete in only a cycle or two. In contrast, the same polymer scanned in PSS can be subjected to large potential excursions without substantial degradation because the extent of the doping process is being limited. Such self-limiting behavior reduces the need for careful potential control in applications that involve the cycling of doping state.

The cycling data of Figure 8 also hint at the quality of the self-limiting behavior achieved. As the potential is swept positive, there is an increasing disagreement between the scan rate normalized voltammograms. The slowest scan rate sweep exhibits the largest value of $I\nu^{-1}$, suggesting a slow background process that relies in some way on the diffusion of a reagent to the film. A likely explanation is the diffusion of small impurity anions in the PSS electrolyte that can support oxidation beyond the self-limited level. Indeed, the shape of the voltammograms at large positive potentials is reminiscent of the tails seen in voltammograms of solution-phase redox couples. This is further seen by normalizing the data by $\nu^{-1/2}$ as is appropriate for the planar diffusion of electroactive species to the electrode surface.[23] Figure 10 shows that data of Figure 8 normalized in such a manner, and there is good agreement in the anodic tail following E_p^{an} in particular in the region after potential reversal (highlighted by rectangle in Figure 8). This is consistent with some doping supported by the diffusion of residual small anion impurities in the PSS electrolyte.

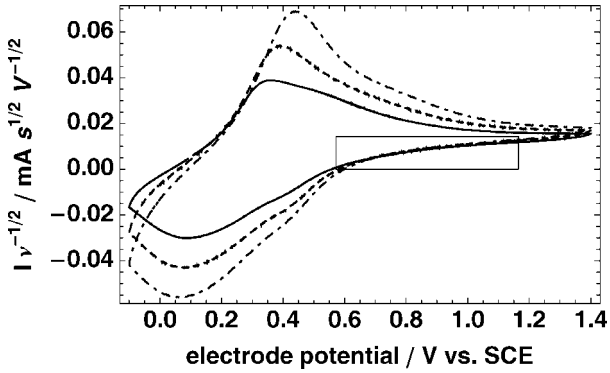

Figure 10. Cyclic voltammograms of Figure 8A replotted with the current (I) normalized by $\nu^{-1/2}$ where ν is the scan rate. The scan rate line type assignments are as in Figure 8A, and the rectangle is to highlight the overlap region in this normalization.

4. Conclusion

A family of polyacetylene anionomers and cationmers have been prepared by the ring-opening metathesis copolymerization of derivatized cyclooctatetraenes. The ionic functional group density could be systematically controlled by variation of the monomer feedstock, and polymers ranging from approximately 1 ion per 5 double bonds to 1 ion per 65 double bonds were prepared. The range of both ionic functional groups densities and charge make this family of materials ideal for exploring fundamental transport issues in ion-containing polymeric semiconductors as well as electroactive interfaces and devices based on them. The electrochemical behavior of the conjugated polymers was found to be a superposition of that of the constituent homopolymers. The ion-rich regions of the polymer could be selectively accessed using SLED. This is a self-limiting method of preparing polymers with precise doping levels without regard to electrode potential, as was explicitly demonstrated for both the n-doping of polyacetylene cationomers and the p-doping of polyacetylene anionomers. The self-limiting nature of SLED was also used to greatly extend the potential stability window of polyacetylene anionomers by limiting the extent of doping to below degradative levels. The reliance of SLED on the built-in ion content of conjugated ionomers to control redox chemistry makes it a powerful tool for controlling the doping chemistry of conjugated polymers.

5. Experimental Section

5.1. Materials. The monomers and tungsten alkylidene were synthesized as described previously.[16,24] Dimethylformamide (DMF, Burdick and Jackson) and DMF-d_7 (Cambridge Isotopes Laboratory) were dried with 4 Å molecular sieve and degassed using three freeze−pump−thaw cycles. Acetonitrile (HPLC grade, Mallinckrodt) was distilled from P_2O_5 before use. Tetramethylammonium tetrafluoroborate ($TMABF_4$, Aldrich) and tetrabutylammonium tetrafluoroborate ($TBABF_4$, Aldrich) were recrystallized from water and ethyl acetate, respectively, and dried at 80 °C under vacuum (20 mTorr) for a minimum of 96 h. Tetrabutylammonium polystyrenesulfonate (PSS) was prepared by ion exchange from sodium polystyrenesulfonate (Scientific Polymer Products, $M_w = 50\,000$). Dowex 50W-X8 (Baker) was charged by sequential washings with (1) 1 M HCl, (2) H_2O, (3) 40% (w/w) tetrabutylammonium hydroxide (Aldrich), and (4) H_2O. Ion exchange was achieved by passage of an aqueous solution of the sodium salt down the charged Dowex column. The resulting tetrabutylammonium salt was dialyzed for several days using Spectra/Por 4 cellulose dialysis membranes and then dried in vacuo (20 mTorr) for 7 days at 80 °C. PDDP was synthesized as previously descibed[19] and dried under vacuum (20 mTorr) at 80 °C for 96 h before use. Benzaldehyde (99.9% redistilled, Aldrich) was used as received.

5.2. Polymerizations. All polymerizations were conducted in a nitrogen-filled glovebox because of the air and moisture sensitivity of the process. Stock solutions of the monomers were made by dissolution in chloroform and stored in the dark. Portions of the stock solutions were combined and diluted to achieve the desired concentration and monomer ratio. A solution of catalyst **1** in chloroform was then added to initiate the polymerizations, and they were terminated at the desired time by the addition of benzaldehyde. The chloroform and unreacted TMSCOT were removed under vacuum, and the remaining solids were then thoroughly washed with acetonitrile to remove excess ionic monomer, catalyst residue, and backbiting products.

5.3. Characterization. NMR spectra were recorded with a Varian INOVA 300 MHz spectrometer with polymer solutions in DMF-d_7. Visible absorption spectroscopy was performed on DMF solutions using a Hewlett-Packard 8452A diode array spectrometer. Gel permeation chromatography was performed on a Waters chromatography system utilizing a Styragel HR4 size exclusion column, a 515 pump, and 2410 differential refractometer. The latter was also used to determine the refractive index increment dn/dc for molecular weight calculations. The flow rate of the GPC was 0.3 mL/min. MALLS was conducted with a Wyatt Technologies Dawn EOS system operating at 788 nm either in line with the GPC system or in batch mode.

5.4. Electrochemical Methods. Cyclic voltammetry was performed with a Solartron 1286 using a standard inert-atmosphere, three-electrode cell with a glassy carbon working electrode, coiled platinum wire counter electrode, and a nonaqueous Ag(s)/Ag^+ reference electrode. The reference electrode was prepared from a 3 mm diameter glass tube fitted at one end with a Vycor frit (Bioanalytical Systems, Inc.) and filled with either 0.075 M $TMABF_4$/0.005 M $AgNO_3$/CH_3CN or 0.1 M $TBABF_4$/0.005 M $AgNO_3$/CH_3CN. The nonaqueous reference electrode was calibrated against a commercial saturated calomel electrode. The glassy carbon electrode was polished with 0.05 μm alumina paste, thoroughly rinsed, and then dried under vacuum (20 mTorr) overnight before use. All electrochemical experiments were conducted using thin polymer films which were deposited on the glassy carbon electrode by drop-casting 10 μL of DMF/polymer solution (1−5 mg mL^{-1}).

Acknowledgment. This work was supported by the National Science Foundation Division of Materials Research (NSF DMR-0519489). The authors thank Carrie Hafer and David Stay for helpful comments.

References and Notes

(1) Pei, Q. B.; Yu, G.; Zhang, C.; Yang, Y.; Heeger, A. J. *Science* **1995**, *269*, 1086–1088.
(2) Baur, J. W.; Kim, S.; Balanda, P. B.; Reynolds, J. R.; Rubner, M. F. *Adv. Mater.* **1998**, *10*, 1452–1455.
(3) Sun, Q.; Li, Y.; Pei, Q. *J. Disp. Technol.* **2007**, *3*, 211–224.
(4) Gao, J.; Yu, G.; Heeger, A. J. *Appl. Phys. Lett.* **1997**, *71*, 1293–1295.
(5) Bernards, D. A.; Flores-Torres, S.; Abruna, H. D.; Malliaras, G. G. *Science* **2006**, *313*, 1416–1419.
(6) Mcquade, D. T.; Pullen, A. E.; Swager, T. M. *Chem. Rev.* **2000**, *100*, 2537–2574.
(7) Pinto, M. R.; Schanze, K. S. *Synthesis* **2002**, 1293–1309.
(8) Gao, J.; Li, Y. F.; Yu, G.; Heeger, A. J. *J. Appl. Phys.* **1999**, *86*, 4594–4599.
(9) Cimrova, V.; Schmidt, W.; Rulkens, R.; Schulze, M.; Meyer, W.; Neher, D. *Adv. Mater.* **1996**, *8*, 585–587.
(10) Edman, L.; Pauchard, M.; Liu, B.; Bazan, G.; Moses, D.; Heeger, A. J. *Appl. Phys. Lett.* **2003**, *82*, 3961–3963.
(11) Edman, L. *Electrochim. Acta* **2005**, *50*, 3878–3885.
(12) Ikenoue, Y.; Chiang, J.; Patil, A. O.; Wudl, F.; Heeger, A. J. *J. Am. Chem. Soc.* **1988**, *110*, 2983–2985.
(13) Ikenoue, Y.; Uotani, N.; Patil, A. O.; Wudl, F.; Heeger, A. J. *Synth. Met.* **1989**, *30*, 305–319.
(14) Klavetter, F. L.; Grubbs, R. H. *J. Am. Chem. Soc.* **1988**, *110*, 7807–7813.

(15) Moore, J. S.; Gorman, C. B.; Grubbs, R. H. *J. Am. Chem. Soc.* **1991**, *113*, 1704–1712.
(16) Gorman, C. B.; Ginsburg, E. J.; Grubbs, R. H. *J. Am. Chem. Soc.* **1993**, *115*, 1397–1409.
(17) Cheng, C. H. W.; Boettcher, S. W.; Johnston, D. H.; Lonergan, M. C. *J. Am. Chem. Soc.* **2004**, *126*, 8666–8667.
(18) Cheng, C. H. W.; Lonergan, M. C. *J. Am. Chem. Soc.* **2004**, *126*, 10536–10537.
(19) Elliott, C. M.; Redepenning, J. G.; Balk, E. M. *J. Am. Chem. Soc.* **1985**, *107*, 8302–8304.
(20) Lonergan, M. C.; Cheng, C. H.; Langsdorf, B. L.; Zhou, X. *J. Am. Chem. Soc.* **2002**, *124*, 690–701.
(21) Salzer, C. A.; Elliott, C. M.; Hendrickson, S. M. *Anal. Chem.* **1999**, *71*, 3677–3683.
(22) Johnson, L. K.; Virgil, S. C.; Grubbs, R. H.; Ziller, J. W. *J. Am. Chem. Soc.* **1990**, *112*, 5384–5385.
(23) Bard, A. J.; Faulkner, L. R. *Electrochemical Methods: Fundamentals and Applications*; Wiley: New York, 1980.
(24) Langsdorf, B. L.; Zhou, X.; Adler, D. H.; Lonergan, M. C. *Macromolecules* **1999**, *32*, 2796–2798.
(25) Schrock, R. R.; Depue, R. T.; Feldman, J.; Schaverien, C. J.; Dewan, J. C.; Liu, A. H. *J. Am. Chem. Soc.* **1988**, *110*, 1423–1435.
(26) Schrock, R. R. *Tetrahedron* **1999**, *55*, 8141–8153.
(27) Langsdorf, B. L.; Zhou, X.; Lonergan, M. C. *Macromolecules* **2001**, *34*, 2450–2458.
(28) Odin, C.; Nechtschein, M. *Phys. Rev. Lett.* **1991**, *67*, 1114–1117.
(29) Odin, C.; Nechtschein, M. *Synth. Met.* **1991**, *44*, 177–188.
(30) Odin, C.; Nechtschein, M.; Hapiot, P. *Synth. Met.* **1992**, *47*, 329–350.
(31) Chien, J. C. W.; Schlenoff, J. B. *Nature (London)* **1984**, *311*, 362–363.
(32) Beck, F.; Braun, P.; Oberst, M. *Ber. Bunsen-Ges. Phys. Chem. Chem. Phys.* **1987**, *91*, 967–974.
(33) Krische, B.; Zagorska, M. *Synth. Met.* **1989**, *28*, C257−C262.
(34) Tsai, E. W.; Basak, S.; Ruiz, J. P.; Reynolds, J. R.; Rajeshwar, K. *J. Electrochem. Soc.* **1989**, *136*, 3683–3689.

MA8004108